Annals of Nuclear Medicine Vol. 19, No. 7, 633–639, 2005

Evaluating performance of a pixel array semiconductor SPECT system for small animal imaging

Naoki KUBO,* Songji ZHAO,***** Yutaka FUJIKI,** Akiyoshi KINDA,*** Nobutoku MOTOMURA,*** Chietsugu KATOH,* Tohru SHIGA,***** Hidekazu KAWASHIMA,**** Yuji KUGE***** and Nagara TAMAKI*****

*Department of Health Sciences, School of Medicine, Hokkaido University
**Acrorad Co. Ltd.
***Toshiba Medical Systems
****Department of Nuclear Medicine and Diagnostic Imaging, Graduate School of Medicine, Kyoto University
*****Graduate School of Medicine, Hokkaido University

Objectives: Small animal imaging has recently been focused on basic nuclear medicine. We have designed and built a small animal SPECT imaging system using a semiconductor camera and a newly designed collimator. We assess the performance of this system for small object imaging. ***Methods:*** We employed an MGC1500 (Acrorad Co.) camera including a CdTe semiconductor. The pixel size was 1.4 mm/pixel. We designed and produced a parallel-hole collimator with 20-mm hole length. Our SPECT system consisted of a semiconductor camera with the subject holder set on an electric rotating stage controlled by a computer. We compared this system with a conventional small animal SPECT system comprising a SPECT-2000H scanner with four Anger type cameras and pinhole collimators. The count rate linearity for estimation of the scatter was evaluated for a pie-chart phantom containing different concentrations of ^{99m}Tc. We measured the FWHM of the ^{99m}Tc SPECT line source along with scatter. The system volume sensitivity was examined using a flood source phantom which was 35 mm long with a 32-mm inside diameter. Additionally, an *in vivo* myocardial perfusion SPECT study was performed with a rat. ***Results:*** With regards to energy resolution, the semiconductor camera (5.6%) was superior to the conventional Anger type camera (9.8%). In the count rate linearity evaluation, the regression lines of the SPECT values were $y = 0.019x + 0.031$ ($r^2 = 0.999$) for our system and $y = 0.018x + 0.060$ ($r^2 = 0.997$) for the conventional system. Thus, the scatter count using the semiconductor camera was less than that using the conventional camera. FWHMs of our system and the conventional system were 2.9 ± 0.1 and 2.0 ± 0.1 mm, respectively. Moreover, the system volume sensitivity of our system [0.51 kcps/(MBq/m*l*)/cm] was superior to that of the conventional system [0.44 kcps/(MBq/m*l*)/cm]. Our system provided clear images of the rat myocardium, sufficient for practical use in small animal imaging. ***Conclusions:*** Our SPECT system, utilizing a semiconductor camera, permits high quantitative analysis by virtue of its low scatter radiation and high sensitivity. Therefore, this system may contribute to molecular imaging of small animals and basic medical research.

Key words: semiconductor detectors, small animal imaging, single photon emission computed tomography

INTRODUCTION

MOLECULAR IMAGING of small animals, such as mice and rats, *in vivo*, is vital in the study of human disease models and will provide important clues on the pathogenesis, progression and treatment of many disorders, and on the characterization of gene expression and phenotype changes that arise from genetic manipulation.[1,2] A typical

Received March 17, 2005, revision accepted July 19, 2005.
For reprint contact: Naoki Kubo, Ph.D., Department of Health Sciences, School of Medicine, Hokkaido University, Kita 12 Nishi 5, Kita-ku, Sapporo 060–0812, JAPAN.
E-mail: naoki@cme.hokudai.ac.jp

radiopharmaceutical study requires animal dissection for organ counting or autoradiography. In comparison, an *in vivo* technique, such as single photon emission computed tomography (SPECT), provides numerous benefits. SPECT imaging can be continuously applied to the same animal over long-duration experiments. Thus, the number of animals needed for *in vivo* techniques is considerably less than the number required for *ex vivo* measurements, in which the animal has to be killed for a single measurement. The smaller number of animals required for an *in vivo* approach is beneficial from an ethical point of view and may also save research time, therefore saving costs.[3] However, for SPECT applications, various physical factors limit the accuracy of quantitative measurements. Among these are the finite spatial resolution and scatter radiation.[4]

Recently, semiconductor-based gamma cameras have become available for sentinel lymph node mapping and/or experiments in radiopharmaceutics.[5,6] The semiconductor camera is superior to Anger-type cameras in spatial resolution, energy resolution and counting efficiency.[7–9] The use of semiconductor cameras for small animal SPECT requires the development of an appropriate collimator. Once such a collimator has been designed, it is hoped that SPECT using semiconductor cameras will contribute to *in vivo* quantitative examinations.

This study reports the design of a collimator for small animal SPECT and the development of a semiconductor-camera SPECT system. The performance of this system was assessed for small object imaging.

MATERIALS AND METHODS

Semiconductor-based gamma camera

We employed an MGC1500 (Acrorad Co. Ltd., Tokyo, Japan) camera consisting of a CdTe semiconductor. The outer dimensions of the camera head were 82 mm × 82 mm × 205 mm, and its weight was 1.4 kg. The field of view was 44.6 mm × 44.6 mm. The CdTe module had 1,024 pixels in 32 rows. Each row consisted of 32 individual elements that had dimensions of 1.4 mm × 1.4 mm and a height of 5 mm. The detector thickness was optimized for detecting 140 keV photons of ^{99m}Tc. The rate of 140-keV energy absorption in a 5-mm thickness of CdTe is theoretically about 88%.[5]

Collimator design

We calculated the theoretical resolution, R, for the original collimator of the MGC1500. This collimator, with a 10-mm hole length was composed of tungsten, having 1.2 mm × 1.2 mm square openings and a septum thickness of 0.2 mm to fit the geometry of the CdTe pixels. The depth from the end-of-hole to the midplane-of-detector was 4.5 mm. The geometric resolution of a parallel-hole collimator can be calculated using the general method described by Anger, which calculates the half height of the response to a point source. In this method the geometric resolution R is given by

$$R = (a_e + b + c)/a_e . \quad \text{Eq. 1}$$

Here a_e is the effective collimator length, which has been reduced from the actual length a because of septum penetration at both ends of the holes, and is given approximately by $a_e = a - 2\mu^{-1}$, where μ^{-1} is the mean free path of gamma rays in the collimator material (140 keV photons in tungsten). Variable b is the distance from the collimator face to the point source and c is the depth from the end-of-hole to the midplane-of-detector.[10,11]

We also calculated the geometric resolution of a collimator that we designed for small animal SPECT. This collimator had a 20-mm hole length and the same values for the other parameters as the original collimator of the MGC1500. Figure 1 shows the calculated geometric resolution. In the SPECT system of this study we used the collimator of our design.

System description

The small animal SPECT system consisted of a semiconductor camera with our collimator and a subject holder on an electric rotating stage (PR-080236, MEIRITSU Co., Yokohama, Japan) controlled by computer (MSC controller MS-C6002, MEIRITSU Co.). To acquire tomographic projection images, the subject was positioned upright in an acrylic tube and rotated around a vertical axis in front of the stationary semiconductor camera.[1,12,13] The acrylic tube had an inner diameter of 45 mm, a thickness of 2 mm and a length of 250 mm. The tube had a slit width of 20 mm. Figure 2 shows an overview of the small animal SPECT system with the semiconductor camera.

Anger-type camera

We compared our system with a conventional small animal SPECT system comprising a SPECT-2000H scanner (Hitachi Medical Co., Tokyo, Japan). This conventional Anger-type system has four scintillators with NaI

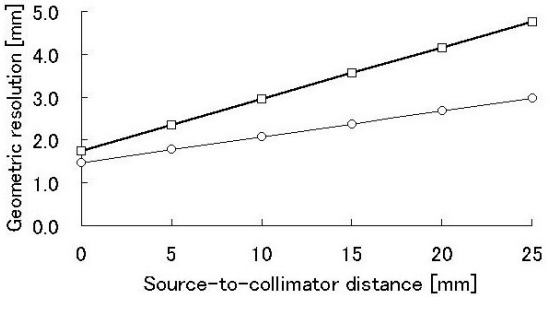

Fig. 1 The calculated geometric resolution of collimators with source-to-collimator distance. The squares indicate the original collimator of the MGC1500. The circles indicate our collimator designed with a 20-mm hole length for small animal SPECT.

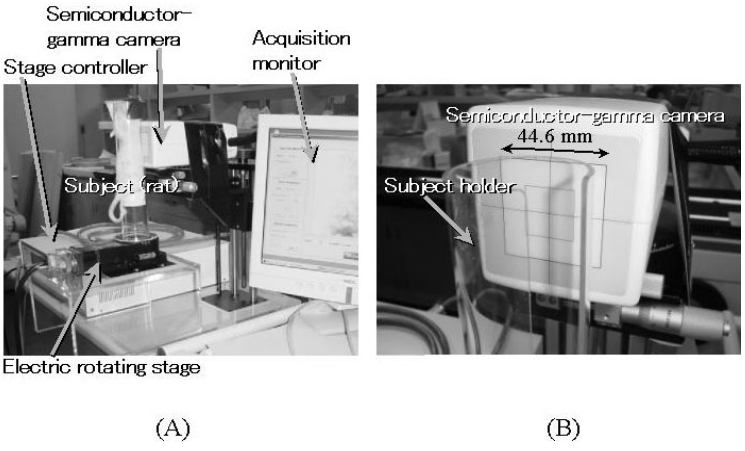

Fig. 2 (A) Overview of the small animal SPECT system with a semiconductor-gamma camera. The camera is equipped with the collimator of our own design. (B) Front view of the semiconductor-gamma camera.

crystals sized 260 mm × 208 mm × 9 mm and 120 photomultiplier tubes. This system consists of four scintillators using tungsten pinholes and lead shields. The effective aperture size of the pinhole was 1.2 mm. The distance from the scintillator to the pinhole was 130 mm and the distance from the pinhole to the axis of rotation was 50 mm.[14]

Line-spread function of the semiconductor camera with different collimators

We acquired and compared line-spread functions of the original collimator for the MGC1500 and for our collimator. A line source of 0.85-mm inner diameter filled with 722 MBq/m*l* ^{99m}Tc was placed in the center of the semiconductor camera. The distance from the surface of the collimator to the line source was 20 mm.

Confirmation of the polarization phenomenon

The polarization phenomenon causes the counting efficiency to decrease. To determine whether the polarization phenomenon occurred, the total count was measured for each SPECT projection frame. The relationship between the total count and the frame number gave the relationship between the count over time in the SPECT acquisition.

Energy resolution

Energy resolutions were measured with a ^{99m}Tc flat source for the semiconductor camera and a ^{99m}Tc point source for the Anger-type cameras. Energy resolution was defined as the full-width at half-maximum (FWHM) of the peak photoresponse divided by its mean amplitude. In the Anger-type cameras, averaging of the four cameras was performed.

Count rate linearity examination with scatter

To examine the count rate linearity, SPECT of a pie chart phantom was performed using the semiconductor camera and the Anger-type camera systems. The pie chart phantom was divided into six cavities, each 2.8 m*l* in volume. The cavity septum had a thickness of 1 mm. The phantom size was 32 mm in diameter and 25 mm in height. Each cavity contained a different concentration of a homogeneous solution of ^{99m}Tc (0, 10, 21, 30, 41 and 52 MBq/m*l*). A circular 5.4-mm diameter region-of-interest (ROI) was placed over each cavity and the SPECT value was calculated. The relation between ^{99m}Tc activity concentration and the SPECT value of each cavity region was fitted to a line using a least squares method.[15] Each SPECT value was normalized to the 52-MBq/m*l* SPECT value. Since a SPECT image includes scatter radiation, the *y*-intercept corresponding to no activity was not zero.

Spatial resolution

Line source SPECT with scatter was performed using a phantom consisting of a water-filled acrylic cylinder with an inside diameter of 32 mm. A line source of 0.85-mm inner diameter filled with 290 MBq/m*l* ^{99m}Tc was placed in the center of the cylinder.

The spatial resolution of SPECT was measured as the FWHM of the line-spread function.[16] FWHMs were measured in the horizontal and vertical directions of the image frame. Simultaneously, the average and standard deviation (SD) of ten axial slices were calculated.

System volume sensitivity

The system volume sensitivity was examined using a flood source phantom. The flood source phantom was a 35-mm-long cylinder with a 32-mm inside diameter. The cylinder was filled with 27 MBq/m*l* ^{99m}Tc uniformly mixed in water. The volume sensitivity per axial centimeter was calculated from the total counts imaged, the total acquisition time and the activity (decay corrected).[16–18] The volume sensitivity was expressed as kcps/(MBq/m*l*)/cm.

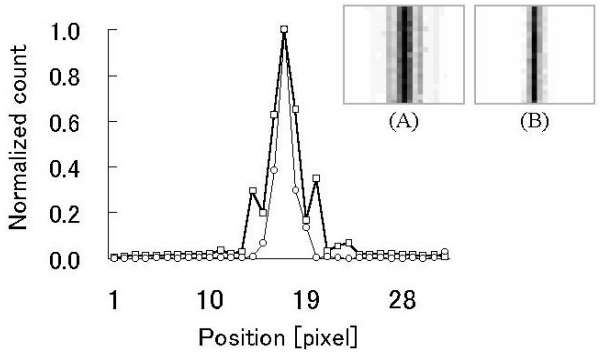

Fig. 3 Line-spread functions at a 20-mm source-to-collimator distance with different collimators. The squares indicate the line-spread function using the original collimator of the MGC1500. The circles show the line-spread function using the collimator of our own design. (A) The line source image using the original collimator of the MGC1500. (B) The line source image using the collimator of our own design.

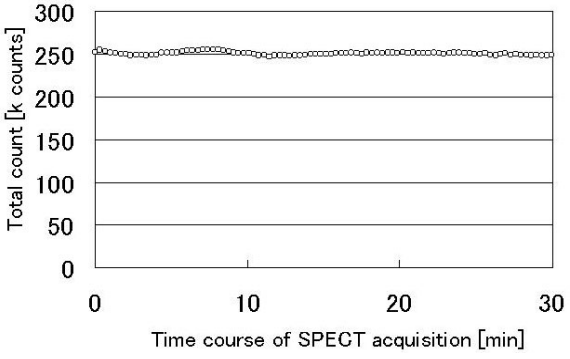

Fig. 4 The total count in each frame of the flood source cylindrical phantom over time in SPECT acquisition corrected for decay.

Small animal brain slice phantom

To evaluate the performance of the semiconductor-camera system, SPECT of a small animal brain slice phantom was performed. The small animal brain slice phantom was 24 mm wide, 16 mm high and 5 mm thick. In this phantom, the lobus parietalis cortex had a thickness of about 3 mm and the longitudinal fissure had a width of 1.3 mm. This phantom contained a homogeneous solution of 132 MBq/m*l* ^{99m}Tc.

In vivo *small animal myocardial perfusion SPECT study*

In the *in vivo* small animal myocardial perfusion SPECT study using the semiconductor-camera system, a rat was used as the subject. The rat had a weight of 210 g. It was anesthetized and imaged 30 minutes after injection of 115 MBq ^{99m}Tc-MIBI. The experiment was performed in accordance with the guidelines for the care and use of laboratory animals of the Hokkaido University Graduate School of Medicine.

SPECT acquisition

In the semiconductor-camera system, the projection data were acquired while continuously rotating the stage, with 90 views over 360° at 20.3 sec/view. The photopeak was centered at 140 keV with a ±10% window. The acrylic tube was close to the semiconductor camera face and therefore the radius of rotation was 22.5 mm.

SPECT data were obtained with the Anger-type cameras using a 128 × 128 acquisition matrix in step-and-shoot mode with 64 steps over 360° at 20 sec/step. The energy window setting was the same as that for the semiconductor camera, 140 keV ± 10%.

SPECT reconstruction

The projection data of the semiconductor camera were entered into the GMS computer system (Toshiba Medical Systems, Tochigi, Japan). The projection data were converted to a 64 × 64 matrix and uniformity correction was performed. A ramp filter was used for reconstructions with filtered backprojection. No scatter or attenuation corrections were performed. A pre-filter was not used for phantoms or line source data. Myocardial projection data were processed using a Butterworth filter with an order of 8 and a critical frequency of 3.57 cycles/cm.

SPECT with the Anger-type cameras did not use a pre-reconstruction filter. The reconstruction method has been previously described in detail by Ishizu and co-workers.[14]

RESULTS

Line-spread functions of the semiconductor camera with different collimators

Figure 3 shows the line-spread functions at a source-to-collimator distance of 20 mm for the original collimator of the MGC1500 and for our collimator. When using the original collimator of the MGC1500, sub peaks as artificial peaks appeared neighboring the main peak. When using our collimator, however, sub peaks were not apparent.

Confirmation of the polarization phenomenon

Figure 4 shows the total count of each projection for the flood source phantom over the elapsed time of SPECT acquisition corrected for decay. The total count was almost constant, with no occurrence of the polarization phenomenon.

Energy resolution

With regards to energy resolution, the semiconductor camera (5.6%) was superior to the conventional Anger-type camera (9.8%).

Count rate linearity examination with scatter

Figure 5 shows SPECT of the pie-chart phantom. The regression lines of the SPECT values were $y = 0.019x + 0.031$ ($r^2 = 0.999$) for our semiconductor system and $y =$

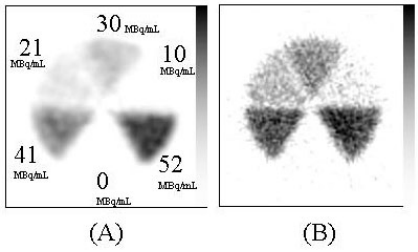

Fig. 5 SPECT of the pie-chart phantom. (A) Transverse SPECT image using the semiconductor-camera system. The effective slice thickness was 0.7 mm because the matrix size was converted from 32 × 32 to 64 × 64. (B) Transverse SPECT image using the conventional Anger-type system. The slice thickness was 0.5 mm.

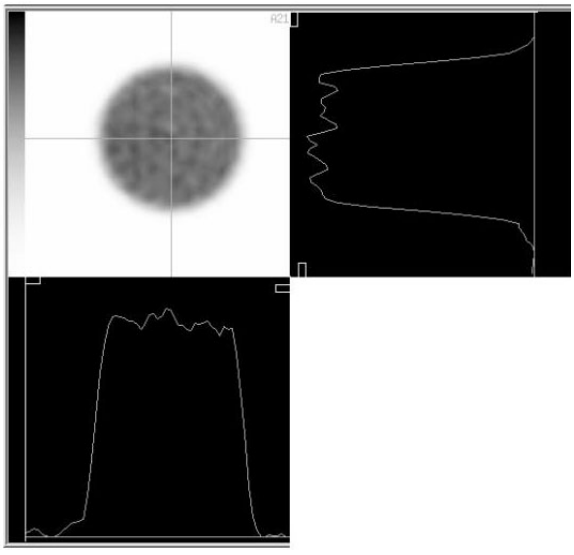

Fig. 6 SPECT of the flood source phantom with a diameter of 32 mm using the semiconductor-camera system. Graphs show profiles in the *x* and *y* directions.

$0.018x + 0.060$ ($r^2 = 0.997$) for the conventional Anger-type system. The *y*-intercept for the semiconductor-camera system was approximately half that for the Anger-type camera system.

Spatial resolution

FWHMs of the semiconductor-camera system and the conventional Anger-type system were 2.9 ± 0.1 and 2.0 ± 0.1 mm, respectively.

System volume sensitivity and flood source phantom SPECT

The system volume sensitivity of the semiconductor-camera system [0.51 kcps/(MBq/m*l*)/cm] was superior to that of the conventional Anger-type system [0.44 kcps/(MBq/m*l*)/cm]. No nonuniformity artifacts were seen in the SPECT of the flood source phantom, as shown in Figure 6.

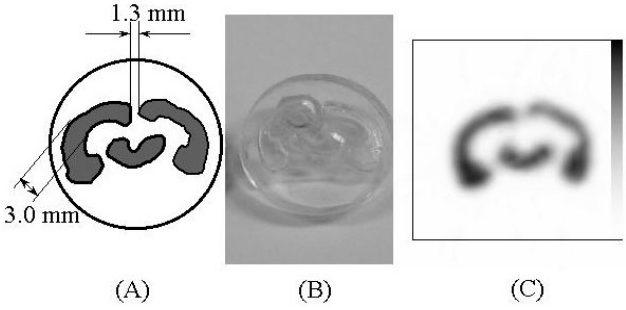

Fig. 7 (A) Schema of small-animal brain slice-phantom. (B) Photograph of the phantom. (C) SPECT of the slice-phantom using the semiconductor-camera system.

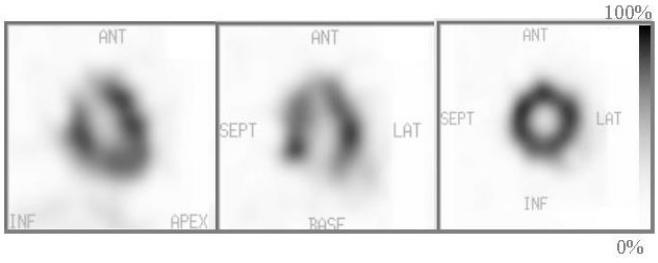

Fig. 8 Myocardial SPECT of the rat (weight: 210 g) in an upright position using the semiconductor-camera system.

Small animal brain slice phantom SPECT

The small animal brain slice phantom was successfully visualized using the semiconductor-camera SPECT system, as shown in Figure 7. In particular, the 1.3-mm cleft was explicitly visualized.

In vivo *small animal myocardial perfusion SPECT study*

SPECT performed on a rat successfully visualized the myocardium *in vivo*, as shown in Figure 8. The background was satisfactorily low. The left ventricle is shown clearly and the image contrast is excellent. Also, no artifacts appear in the SPECT images. Therefore, myocardial SPECT in a normal rat can be visualized with the normal distribution of ^{99m}Tc-MIBI.

DISCUSSION

We have built a small animal SPECT imaging system using a commercial semiconductor camera. We have designed a collimator with a hole length of 20 mm for small object SPECT. This system was shown to be suitable for SPECT with a small field of view of 45 mm. The most exceptional feature of this system is its compact size. All components of this system can fit on a desktop. Therefore, this system can be applied in a small laboratory.

Line-spread functions of the semiconductor camera with different collimators

Using the original collimator of the MGC1500, sub peaks appeared as artificial peaks neighboring the main peak. Since the original collimator had a short hole length, the acceptance angle of the hole was wide, increasing the distance from the collimator to source. Consequently, the holes in the neighborhood of the main peak accept gamma rays which are emitted obliquely. If sub peaks appear in the same position in the field-of-view of the camera, ring artifacts are produced in SPECT. Using our collimator, sub peaks did not appear. Therefore, SPECT using our collimator has no ring artifacts.

Polarization

Polarization is the major problem in semiconductor detectors. Polarization induces a decrease in the thickness of the space charge in semiconductor detectors. Accordingly, the counting rate and charge-collection efficiency are decreased.[19] In this study, the total count of each projection for the flood source phantom was almost constant. Also, it was considered that non-attenuation of radiation through the acrylic tube slit accounted for a slight deviation in the total count. Thus, the polarization phenomenon was not observed during a 30-minute acquisition, a substantial time for SPECT examination.

Energy resolution and count rate linearity examination with scatter

The scatter count of SPECT using the semiconductor camera was less than that using the Anger-type camera. Semiconductors allow the direct conversion of absorbed energy to an electric charge, which leads to a much better energy resolution as compared to scintillator-based systems.[7] Improvement in the detector energy resolution reduces the scatter count and correspondingly improves the quantitative accuracy of the SPECT measurements.[4] Heanue demonstrated that an energy resolution of 3–4 keV is sufficient to render the error due to scatter insignificant compared to the uncertainty due to photon statistics in a 15-cm radius water-filled cylinder.[4] To date, semiconductor cameras have not achieved an energy resolution this high. In the near future, when highly efficient cooling equipment is installed on semiconductor cameras for detector chilling, the energy resolution will greatly improve. Thus, semiconductor detectors hold great promise for the future.

Spatial resolution using our collimator and SPECT images

The finite spatial resolution of the system influences quantitative analysis using SPECT imaging due to the partial volume effect.[20–22] As SPECT systems improve, they will be able to perform high precision quantitative analysis. Segmentation of the detectors into pixel arrays with very fine pitch allows a high spatial resolution.[7,23–26] Importantly, a collimator that allows such a high spatial resolution is also required. Hence, we designed a collimator for small animal SPECT and were consequently able to achieve a spatial resolution approaching that of the conventional small animal SPECT system.

An intrinsic property in digital imaging is the shifted-alignment. A shifted-alignment occurs when the center of the point source coincides with the edge of the pixel. In this case, the point source extends over two pixels.[25,27] This phenomenon can even arise at a source-to-collimator distance of 0 mm. In calculations based on our collimator (a hole length of 20 mm), the geometric resolution at a source-to-collimator distance of 22.5 mm was determined to be smaller than the length of two pixels. Thus, the extent of shifted-alignment for a point source at the center of rotation for our system was almost equal to that at a distance of 0 mm. We believe that this resolution for the center of rotation is acceptable.

The spatial resolution and sensitivity are inverse to each other with respect to the hole length of a parallel collimator. As the hole length increases, the sensitivity decreases. To avoid compromising sensitivity in small animal SPECT, we produced a collimator with a 20-mm hole length rather than a greater hole length.

Semiconductor cameras have thinner detectors than those of Anger-type cameras.[5–7] This property contributes to a high spatial resolution, as shown by Eq. 1. In this study, the spatial resolution of the conventional Anger-type camera was superior to that of the semiconductor camera. The reason was the effect of geometric magnification using pinhole collimators.

Paras et al. determined that the FWHM of a SPECT image is equal to 1.75 times the minimum resolvable hole spacing.[28] Since the FWHM was 2.9 mm for SPECT in this study, the 1.3-mm cleft of the brain slice phantom could be visualized. As shown, the myocardium of the rat subject could be clearly visualized and the left ventricle was explicitly resolved.

Sensitivity

The greater sensitivity of the single semiconductor-camera over the four pinhole Anger-type camera is a particular advantage. This is mainly attributable to use of a parallel-hole collimator with the semiconductor camera. The high sensitivity of the small animal SPECT systems reduces statistical noise. This effect also contributes to an improvement in the quantitative accuracy of the SPECT measurements.

Uniformity

The uniformity of the semiconductor camera is still variable. Therefore, data for uniformity corrections must be acquired every day. In semiconductor cameras, dead pixels and black out pixels rarely arise.[5] However, when they were encountered, the image was reacquired. Semiconductor cameras have improved in recent times, and it

is expected that dead pixels and black out pixels will not occur in new semiconductor cameras.

In conclusion, we have built a compact system for small animal SPECT using a commercial semiconductor camera and a collimator of our design. This SPECT system allows high precision quantitative analysis by virtue of its low scatter radiation and high sensitivity. This system could therefore contribute to molecular imaging of small animals and fundamental medical research.

ACKNOWLEDGMENTS

This study was supported in part by a Grant-in-Aid for Exploratory Research 15659274, from the Ministry of Education, Culture, Sports, Science and Technology (MEXT). The authors are grateful to the Central Institute of Isotope Science, Hokkaido University, for supporting this work.

REFERENCES

1. Loudos GK, Nikita KS, Giokaris ND, Styliaris E, Archimandritis SC, Varvarigou AD, et al. A 3D high-resolution gamma camera for radiopharmaceutical studies with small animals. *Appl Radiat Isot* 2003; 58 (4): 501–508.
2. Acton PD, Kung HF. Small animal imaging with high resolution single photon emission tomography. *Nucl Med Biol* 2003; 30 (8): 889–895.
3. Habraken JB, de Bruin K, Shehata M, Booij J, Bennink R, van Eck Smit BL, et al. Evaluation of high-resolution pinhole SPECT using a small rotating animal. *J Nucl Med* 2001; 42 (12): 1863–1869.
4. Heanue JA, Brown JK, Tang HR, Hasegawa BH. A bound on the energy resolution required for quantitative SPECT. *Med Phys* 1996; 23 (1): 169–173.
5. Tsuchimochi M, Sakahara H, Hayama K, Funaki M, Ohno R, Shirahata T, et al. A prototype small CdTe gamma camera for radioguided surgery and other imaging applications. *Eur J Nucl Med Mol Imaging* 2003; 30 (12): 1605–1614.
6. Abe A, Takahashi N, Lee J, Oka T, Shizukuishi K, Kikuchi T, et al. Performance evaluation of a hand-held, semiconductor (CdZnTe)-based gamma camera. *Eur J Nucl Med Mol Imaging* 2003; 30 (6): 805–811.
7. Darambara DG, Todd-Pokropek A. Solid state detectors in nuclear medicine. *Q J Nucl Med* 2002; 46 (1): 3–7.
8. Mori I, Takayama T, Motomura N. The CdTe detector module and its imaging performance. *Ann Nucl Med* 2001; 15 (6): 487–494.
9. Mueller B, O'Connor MK, Blevis I, Rhodes DJ, Smith R, Collins DA, et al. Evaluation of a small cadmium zinc telluride detector for scintimammography. *J Nucl Med* 2003; 44 (4): 602–609.
10. Anger HO. Scintillation camera with multichannel collimators. *J Nucl Med* 1964; 5: 515–531.
11. Moyer RA. A low-energy multihole converging collimator compared with a pinhole collimator. *J Nucl Med* 1974; 15 (2): 59–64.
12. Wu MC, Gao DW, Sievers RE, Lee RJ, Hasegawa BH, Dae MW. Pinhole single-photon emission computed tomography for myocardial perfusion imaging of mice. *J Am Coll Cardiol* 2003; 42 (3): 576–582.
13. Wu MC, Hasegawa BH, Dae MW. Performance evaluation of a pinhole SPECT system for myocardial perfusion imaging of mice. *Med Phys* 2002; 29 (12): 2830–2839.
14. Ishizu K, Mukai T, Yonekura Y, Pagani M, Fujita T, Magata Y, et al. Ultra-high resolution SPECT system using four pinhole collimators for small animal studies. *J Nucl Med* 1995; 36 (12): 2282–2287.
15. Shinohara H, Yamamoto T, Kuniyasu Y, Hashimoto T, Yokoi T. Implementation and quantitative evaluation of analytical methods for attenuation correction in SPECT: a phantom study. *Phys Med Biol* 1999; 44 (10): 2643–2655.
16. Performance Measurements of Scintillation Cameras. Standards Publication. *National Electrical Manufacturers Association (NEMA)* 2001; NoNU 1.
17. Kouris K, Jarritt PH, Costa DC, Ell PJ. Physical assessment of the GE/CGR Neurocam and comparison with a single rotating gamma-camera. *Eur J Nucl Med* 1992; 19 (4): 236–242.
18. Kouris K, Clarke GA, Jarritt PH, Townsend CE, Thomas SN. Physical performance evaluation of the Toshiba GCA-9300A triple-headed system. *J Nucl Med* 1993; 34 (10): 1778–1789.
19. Bell RO, Entine G, Serreze HB. Time-dependent polarization of CdTe gamma-ray detectors. *Nucl Instrum Meth* 1974; 117: 267–271.
20. Kojima A, Matsumoto M, Takahashi M, Hirota Y, Yoshida H. Effect of spatial resolution on SPECT quantification values. *J Nucl Med* 1989; 30 (4): 508–514.
21. Zito F, Gilardi MC, Magnani P, Fazio F. Single-photon emission tomographic quantification in spherical objects: effects of object size and background. *Eur J Nucl Med* 1996; 23 (3): 263–271.
22. Hoffman EJ, Huang SC, Phelps ME. Quantitation in positron emission computed tomography: 1. Effect of object size. *J Comput Assist Tomogr* 1979; 3 (3): 299–308.
23. Kubo N, Arai H, Shiga T, Katoh C, Tamaki N. Evaluation of a digital scintillator-photodiode camera with a converging collimator for high-resolution imaging. *J Nucl Med* 2003; 44 (5): 1010 Suppl S.
24. Kubo N, Mabuchi M, Arai H, Shiga T, Morita K, Katoh C, et al. Assessment of regional LV function by a digital scintillator-photodiode camera with rotating chair system from gated myocardial SPECT: A study of dynamic myocardial phantom. *J Nucl Med* 2003; 44 (5): 1037 Suppl S.
25. Kubo N, Mabuchi M, Katoh C, Arai H, Morita K, Tsukamoto E, et al. Validation of left ventricular function from gated single photon computed emission tomography by using a scintillator-photodiode camera: a dynamic myocardial phantom study. *Nucl Med Commun* 2002; 23 (7): 639–643.
26. Ketchum LE. New equipment in nuclear medicine, part 1: solid-state detectors. *J Nucl Med* 1998; 39 (11): 15N 35N–15N 36N.
27. Fujita H, Doi K, Giger ML. Investigation of basic imaging properties in digital radiography. 6. MTFs of II-TV digital imaging systems. *Med Phys* 1985; 12 (6): 713–720.
28. Paras P, Hine GJ, Adams R. Latest developments in gamma-camera performance testing: resolution measurements. In: Raynaud C, ed. *Nuclear medicine and biology*. Paris; Pergamon Press, 1982: 2890–2894.